Supporting Information

Nahrendorf et al. 10.1073/pnas.0915163107

SI Methods

Nanoparticle Preparation. Dextran-coated iron oxide nanoparticles (CLIO-47; Center for Systems Biology) served as starting materials. One CLIO nanoparticle contains an average of 2,064 Fe atoms (3.48×10^{-21} mol Fe/particle) (1). The dextran coating of the nanoparticle was crosslinked with epichlorin hydrin, aminated, and labeled with the near-infrared fluorochrome Vivotag-680 (VT680; VisEn Medical) to render particles fluorescent. The ratio of VT680 per nanoparticle was ~5 fluorochromes/particle.

A click labeling strategy was used for ^{18}F-labeling of nanoparticles (2). In brief, nanoparticles were derivatized with alkyne, and the click partner azide was attached to an ^{18}F-labeled polyethylene glycol (^{18}F-PEG$_3$N$_3$). Specifically, 4-pentynoic acid (0.5 g, 5.1 mmol) was converted to the *N*-hydrosuccinimidyl ester by treatment with 1-ethyl-3-(3-dimethylaminopropyl)carbodiimide (1.2 g, 6.4 mmol) and *N*-hydroxysuccinimide (0.7 g, 6.4 mmol) in methylene chloride for 2 h. The mixture was partially concentrated under reduced pressure and subjected to column chromatography (silica gel, 2:3 hexanes: ethyl acetate) providing 0.85 g (an 85% yield) of *N*-succinimidyl 4-pentynoate. ^{1}H NMR (400 MHz; $CDCl_3$) δ: 2.88 (*m*, 6 H), 2.61 (*dt*, *J* = 2.6 Hz, *J* = 7.1 Hz, 2 H), 2.05 (*t*, *J* = 2.6 Hz, ^{1}H). ^{13}C NMR (100 MHz, $CDCl_3$) δ: 169.2, 167.3, 81.1, 70.3, 30.5, 25.8, 14.3. Amidation of aminated CLIO-VT680 with *N*-succinimidyl 4-pentynoate was performed as described previously (3). After size-exclusion chromatography, final alkyne-modified CLIO-VT680 solutions were 1 mg/100 μL in 1× PBS.

The preparation of the 2-(2-(2-azidoethoxy)ethoxy)ethyl *p*-toluenesulfonate precursor began with 2-(2-(2-chloroethoxy)ethoxy) ethanol by reaction with sodium azide (1.1 mol eq) in DMF at 80 °C for 24 h, securing 2-(2-(2-azidoethoxy)ethoxy)ethanol in 92% yield. ^{1}H NMR (400 MHz; $CDCl_3$) δ: 3.74 (*t*, *J* = 4.5 Hz, 2 H), 3.68 (*t*, 6 H), 3.61 (*t*, *J* = 4.6 Hz, 2 H), 3.40 (*t*, *J* = 4.8 Hz, 2 H). ^{13}C NMR (100 MHz, $CDCl_3$) δ: 72.4, 70.6, 70.3, 70.0, 61.7, 50.6. Reaction of this azido PEG$_3$ with tosyl chloride (1.2 mol eq) in the presence of triethyl amine in THF for 2 h provided TsPEG$_3$N$_3$ in 90% yield. ^{1}H NMR (400 MHz; $CDCl_3$) δ: 7.77 (d, J = 8.2 Hz, 2H), 7.32 (d, J = 8.1 Hz, 2H), 4.13 (t, J = 4.7 Hz, 2H), 3.67 (t, J = 5.0 Hz, 2H), 3.61 (t, J = 4.9 Hz, ^{1}H), 3.58 (s, 4H), 3.34 (t, J = 5.0 Hz, 2H), 2.42 (s, 3H). ^{13}C NMR (100 MHz, $CDCl_3$) δ: 144.8, 129.8, 127.9, 70.7, 70.6, 70.0, 69.2, 68.7, 50.6, 21.6. 1-Azido-2-(2-(2-(10)-fluoroethoxy) ethoxy)ethane (^{18}F-PEG$_3$N$_3$) was prepared in 56% ± 3% (n = 5) average decay-corrected radiochemical yield. Analytical HPLC demonstrated >99% radiochemical purity of ^{18}F-PEG$_3$N$_3$. Finally, ^{18}F-PEG$_3$-N$_3$ was conjugated to alkyne-modified CLIO-VT680 nanoparticles using copper-catalyzed azide alkyne cycloaddition chemistry (2). HPLC analysis showed ^{18}F-CLIO-VT680 to be >98% radiochemically pure. ^{64}Cu-CLIO-VT680 was prepared as described previously (4). In brief, CLIO-47 was incubated with dianhydride DTPA (Sigma-Aldrich) for 2 h at room temperature and then purified with a PD-10 column. Here 100 μg of DTPA-NP was used for the labeling with $^{64}CuCl_2$ (equivalent to ~185 MBq ^{64}Cu) in ammonium acetate buffer.

PET-CT Acquisition and Reconstruction. Each PET acquisition was ~80 min in duration. The PET was reconstructed from 600 million coincidental, 511-keV photon counts on a series of lutetium oxyorthosilicate scintillating crystal rings. Counts were rebinned in 3D by registering photons spanning no more than three consecutive rings, then reconstructed into sinograms using a high-resolution Fourier Rebin algorithm. A reconstruction of sinograms yielded a 3D mapping of positron signals using a 2D filtered back-projection algorithm, with a Ramp filter at a Nyquist cutoff of 0.5. Image pixel size was anisotropic, with dimensions of 0.796 mm in the *z* direction and 0.861 mm in the *x* and *y* directions, for a total of 128 × 128 × 159 pixels. Calibration of the PET signal preceded all scans and was done by scanning an 8.0-cm cylindrical phantom containing a known amount of ^{18}F isotope. In PET, Compton scattering has a significant effect and poses a problem in counting true coincident photons from positron-electron annihilation. In the system used, this effect is compensated for by counting only photon energies of 250–750 keV and with a time lapse of <4.1 ns (5). The peak absolute sensitivity of the Inveon PET is ≥10% (percentage of emitted photons detected by PET) (6).

The CT image was reconstructed from 360 projections of x-rays with a cone beam angle of 9.3 degrees over 360 degrees perpendicular to the animal bed. The 80-keV x-rays were transmitted from a 500-μA anode source, 347 mm from the center of rotation, and recorded on a CCD detector containing 2,048 transaxial pixels and 3,072 axial pixels. Projections were calibrated using 70 dark images and 70 light images, interpolated bilinearly, processed through a Shepp-Logan filter, and then reconstructed using a filtered back-projection algorithm. The isotropic CT pixel size was 110.6 μm, with a total of 512 × 512 × 768 pixels. Scaling to Hounsfield units, calibration was done using an 8.0-cm cylindrical phantom containing water before CT acquisition.

FMT Acquisition and Reconstruction. PET, CT, and FMT imaging was done while the anesthetized mice were restrained in a dedicated multimodal imaging cassette (dimensions 50 × 30 × 280 mm; VisEn Medical). The nontransparent body of the cassette has an adjustable height to accommodate mice of different sizes and holds two transparent acrylic windows that allow laser excitation and photon emission in transillumination geometry during FMT imaging. The body is made of carbon and has been tested in MR, PET and CT imaging, where it caused no major artifacts. The fiducial landmarks are positioned on the frame next to the optical windows within the field of view of respective modalities. They can be filled with fluid or gel containing reporter molecules for each given modality. On CT images, they were identified as air-filled holes with lower density compared with the casing (yellow arrows in Fig. 1*C*).

Before imaging, mice were shaved and depilated to remove all hair within the imaging region, because dark hair can absorb light and interfere with optical imaging. Mice were anesthetized (isoflurane 1.5%, O_2 2L/min) during imaging. An isoflurane delivery system is integrated into the multimodal imaging cassette. We acquired 30 frontal slices of 0.5 mm thickness in the *z* direction, with an in-plane resolution of 1 × 1 mm.

After image acquisition, datasets were postprocessed using a normalized Born forward equation to calculate fluorochrome concentration, expressed in nM fluorescence per voxel, as described previously (7–12). In brief, the reconstruction procedure in a typical optical tomography problem consists of solving the inverse problem,

$$\phi_{sc}(r, r_s) = \sum_{n=1}^{N} W(r, r_n, r_s) O(r_n),$$

where $W(r,r_n,r_s)$ represents a weight matrix that associates the effect of the optical property $O(r_n)$ at position r_n with respect to a fluorescence measurement obtained at position r after excitation from a source located at position r_s. Collecting a number of measurements equal to M then allows one to build a system of linear equations giving rise to a matrix equation $y = Wx$, where x corresponds to the distribution $O(r_n)$ of the optical properties in each of the N voxels. W is the total weight matrix that maps the vector containing the fluorochrome concentrations within the imaged sample into the corre-

sponding measurement vector, y. The inversion of the matrix equation provides the unknown fluorophore distribution, x, within the sample. The solution of the inverse problem can be obtained using the diffusion equation, an approximation of the equation of radiative transfer, as a forward model for the light propagation. Information on the geometry of the imaging chamber and the average optical parameters for both the excitation and emission wavelengths is required as well. Implementation of this algorithm corrects for photon scatter and absorption at the expense of spatial resolution, and thus enables fully quantitative, whole mouse tomography.

Multichannel Fusion Software. The open-source software OsiriX was used to view DICOM series. The native OsiriX has some limitations for fusion operation, however; for example, registration of series from different studies can be performed for only two series without losing source pixel values. Thus, we developed a new plug-in, "CSB_Multi_Fusion," to enable fusion of an arbitrary number of series and also to make the process more automated.

The plug-in was designed to modify the native OsiriX viewer controller methods to allow process chains of fused series instead of just one pair. These new methods provide two ways of using multiseries fusion: (*i*) All currently open OsiriX viewer series can be fused immediately, and (*ii*) fusion of series one by one can be performed with drag-and-drop at any time on user request. Because datasets may come from different modalities with profound differences in image parameters (e.g., plane spatial resolution, slice thickness, and number of slices), coregistration and resampling are required. The plug-in relies on the OsiriX native point-based registration.

The algorithm for fusing N series is as follows:

Step 0: User opens N series, marks fiducials ("2D points" by OsiriX's definition) in each series for registration, and starts the plug-in.

Step 1: Register (series 1) and (series 2) and fuse to create a new (series 2),

$$[S_2 -] = [S_1] + [S_2].$$

Step 2:

$$[S_3 -] = [S_3] + [S_2 -] = [S_3] + [S_2] + [S_1].$$

Step N-1: Register and fuse current (series N-1) and (series N),

$$[S_n -] = [S_n] + [S_{n-1} -] = \sum_{i-1}^{N-1} [S_1].$$

In the context of an OsiriX application, "registration of two series" means that the viewer recalculates appropriate series windows in the same coordinate system and with the same voxel size, harmonizing all registered series for image orientation, width, height, and slice thickness.

In the native OsiriX image viewer, screen images can have no more than four bytes per pixel. Most datasets are stored in a monochrome gray-scale format with a depth of 16 bits per pixel. As a result, the fusion of three or more such series is impossible. Thus, we implemented color lookup tables (CLUTs) to differentiate one monochrome series from another. The plug-in constructs several default 16-bit CLUTs and allows users to apply their own custom CLUTs. Only images that are in window memory buffers are processed, keeping the original pixel values of source datasets. Interactive changes of window level or window width (i.e., image intensity), as well as CLUT changes, are applied to all windows currently displayed on the screen. The limit on the number of fused series is defined only by the available RAM size and depends on the dimensions of fused series (pixel width, pixel height, and number of images).

The plug-in was written in Objective-C programming language in XCode 3.1.2 under MacOS 10.5. OsiriX v3.5.1 and ITK (Insight Segmentation and Registration Toolkit) libraries were used for the compilations. A screenshot and a cartoon of quintuple fusion are shown in Fig. 1*C*. In this experiment, a mouse was injected s.c. in different locations with 0.1 nmol of four fluorochomes: AF633 (Invitrogen), VT680, VT750 (Visen Medical), and AF790 (Invitrogen). Immediately thereafter, the mouse was positioned in the multimodal imaging cartridge and imaged with CT and four FMT channels (excitation/emission, 635/655 nm, 680/700 nm, 750/780 nm, and 785/815 nm). The mouse was anesthetized during injection and imaging. FMT and CT data were then fused with the described plug-in (Fig. 1*C*).

Histology. Tissue was embedded in OCT medium (Sakura Finetek), and 6-μm-thick sections were cut. The fluorescent probes were visualized in their respective wavelength, and images were recorded on an upright multicolor Eclipse 80i fluorescent microscope (Nikon) with a mounted CCD camera interfaced to an Apple G5 workstation. Images of different wavelengths were fused using Scanalytics software (BD Biosciences).

Flow Cytometry. The cellular distribution of nanoparticles was assessed by flow cytometry as described previously (4, 13). In brief, blood was drawn 24 h after injection of 15 mg/kg of CLIO-VT680 by cardiac puncture and treated with an ACK buffer [0.15 M NH_4Cl, 10 mM KHCO3, and 0.1 mM Na_2-EDTA (pH 7.3)] to lyse red blood cells. Cells were then labeled with anti-CD11b-APC, lineage markers (anti-CD90-PE, B220-PE, CD49b-PE, NK1.1-PE, and Ly-6G-PE) and anti-F4/80-biotin, I-A^b-biotin, and CD11c -biotin, revealed with streptavidin-PerCP (all from BD Biosciences) for 30 min and analyzed with an LSRII flow cytometer (BD Biosciences). Excitation and detection of the VT680 fluorochrome used a red helium-neon 635-nm laser and a filter combination of 685/LP and 695/40BP.

1. Josephson L, Kircher MF, Mahmood U, Tang Y, Weissleder R (2002) Near-infrared fluorescent nanoparticles as combined MR/optical imaging probes. *Bioconjug* 13: 554–560.
2. Devaraj NK, Keliher EJ, Thurber GM, Nahrendorf M, Weissleder R (2009) ^{18}F-labeled nanoparticles for in vivo PET-CT imaging. *Bioconjug Chem* 20:397–401.
3. Weissleder R, Kelly K, Sun EY, Shtatland T, Josephson L (2005) Cell-specific targeting of nanoparticles by multivalent attachment of small molecules. *Nat Biotechnol* 23: 1418–1423.
4. Nahrendorf M, et al. (2008) Nanoparticle PET-CT imaging of macrophages in inflammatory atherosclerosis. *Circulation* 117:379–387.
5. Constantinescu CC, Mukherjee J (2009) Performance evaluation of an Inveon PET preclinical scanner. *Phys Med Biol* 54:2885–2899.
6. Visser EP, et al. (2009) Spatial resolution and sensitivity of the Inveon small-animal PET scanner. *J Nucl Med* 50:139–147.
7. Vinegoni C, et al. (2009) Born normalization for fluorescence optical projection tomography for whole heart imaging. *J Vis Exp* 28:1389.
8. Vinegoni C, et al. (2009) Normalized born ratio for fluorescence optical projection tomography. *Opt Lett* 34:319–321.
9. Ntziachristos V, Weissleder R (2001) Experimental three-dimensional fluorescence reconstruction of diffuse media by use of a normalized Born approximation. *Opt Lett* 26:893–895.
10. Ntziachristos V, Ripoll J, Wang LV, Weissleder R (2005) Looking and listening to light: the evolution of whole-body photonic imaging. *Nat Biotechnol* 23:313–320.
11. Weissleder R, Ntziachristos V (2003) Shedding light onto live molecular targets. *Nat Med* 9:123–128.
12. Ntziachristos V, Tung CH, Bremer C, Weissleder R (2002) Fluorescence molecular tomography resolves protease activity in vivo. *Nat Med* 8:757–760.
13. Leimgruber A, et al. (2009) Behavior of endogenous tumor-associated macrophages assessed in vivo using a functionalized nanoparticle. *Neoplasia* 11:459–468, 2, 468.

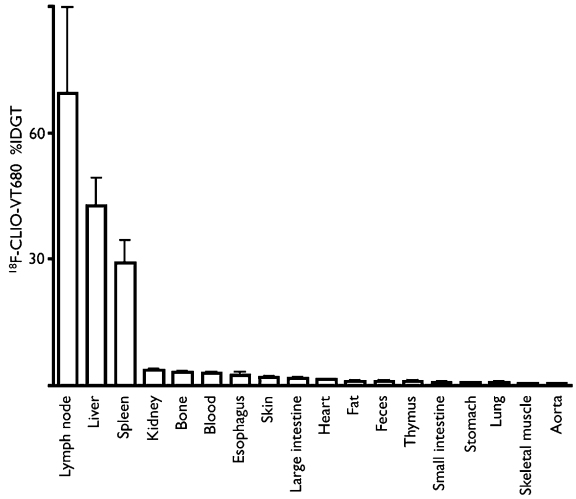

Fig. S1. Biodistribution of ^{18}F-CLIO-VT680 in five control mice 4 h after i.v. injection showing uptake predominantly in the lymphatic system (lymph nodes, spleen) and liver.

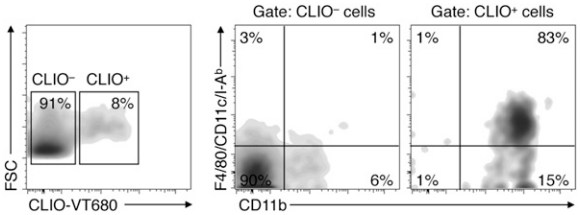

Fig. S2. Cellular uptake profile of CLIO-VT680 was assessed by flow cytometry in three mice at 24 h postinjection. (*Left*) 8% of all live cells in blood took up the nanoparticle. SSC, side scatter. (*Right*) 83% of cells that took up the probe expressed the surface markers CD11b, F4/80, CD11c, and IA^b, indicating that the nanoparticle targeted primarily macrophages and/or dendritic cells. 15% of the CLIO-positive cells were neutrophils [$CD11b^+$ ($F4/80/IA^b/CD11c)^-$].